Article

Spatiotemporal Changes in Air Temperature and Precipitation Extremes over Iran

Mohammad Jamali [1], Alireza Gohari [1], Armita Motamedi [1] and Ali Torabi Haghighi [2,*]

[1] Department of Irrigation, College of Agriculture, Isfahan University of Technology, Isfahan 84156-83111, Iran
[2] Water, Energy and Environmental Engineering Research Unit, University of Oulu, P.O. Box 4300, FIN-90014 Oulu, Finland
* Correspondence: ali.torabihaghighi@oulu.fi

Abstract: In this study, a comprehensive trend analysis was employed to study the spatiotemporal changes in precipitation characteristics with air temperature increasing over time. The nonparametric Mann–Kendall test and the quantile regression methods were applied to detect the plausible temporal trends in 11 extreme rainfall indices and three air temperature indices employed in this study. The results showed there was little evidence to suggest that increases in the maximum of 3-h and 24-h precipitation at higher temperatures resulted in similar increases in the annual precipitation, with most stations throughout Iran showing drying features with higher temperatures. Generally, most regions over Iran scaled negatively, implying a reduction in the annual precipitation ranging from -2.64 to -0.44 mm/°C at higher temperatures. The linear tendencies of the maximum 24-h precipitation ranged from -0.4 to 0.23 mm/°C. The annual precipitation of the stations located at Urmia Lake, Caspian Sea, and the Eastern Border Basins showed a decreasing trend (-3.70 to 1.11 mm/year), while the number of rainy days increased (-2.78 to 4.72), which showed the occurrence of lighter rainfall in these regions. The increasing trend in the maximum 24-h precipitation over Western and Central Iran implied a higher probability of extreme precipitation with a higher intensity. This study revealed that the shift in precipitation extremes shifted from fall to winter by increasing the elevation, but these effects have no statistical significance in Iran.

Keywords: extreme precipitation; global warming; Mann–Kendall test; quantile regression; Iran

1. Introduction

Climate extremes generally refer to the occurrence of climate variables above (below) a certain threshold near the upper (lower) end of its observed range [1]. Extreme events such as extreme precipitation can lead to substantial damage to agriculture, ecology, and infrastructure, as the frequency and intensity of such extremes have increased during the last two decades [2]. Global climate change causes significant changes in the main characteristics of extreme precipitation due to higher evapotranspiration and water vapor amounts in the atmosphere, with several implications for the global hydrological cycle [3,4]. Given the central role of precipitation in the water cycle, the spatiotemporal analysis of extreme precipitation is crucial to enhancing the resilience of socioecological systems and their infrastructure under climate change [5]. The investigation of the main characteristics of extreme precipitation, as well as its spatiotemporal change and trend, has received growing attention in recent decades [6–22]. It is also notable that, except trends in climate precipitation (variability), future climate change has raised the concern of the scientific community. The most advanced tool for future climate projection is regional climate models (RCMs), and their spatial resolution highly affects their accuracy, especially in areas with complex terrain, as depicted in recent studies [23].

Global observations reported a worldwide increase in extreme precipitation [24,25]. The authors of [26] reported that the annual maximum precipitation increased by 65% from

1951 to 1999 on a global scale. The intensity of the annual maximum daily precipitation for nearly two-thirds of rain gauge stations worldwide increased from 1900 to 2009 [27]. Moreover, the intensity of sub-daily extreme rainfall is expected to increase during the coming decades [28].

The spatiotemporal extent and destructive impacts of extreme weather events have undergone tangible changes during the recent decades in arid and semi-arid regions such as Iran. Given that climate and land use are the main drivers of flash flooding, most recent floods can be attributed to changes in extreme precipitation and land cover over Iran. Many studies have analyzed the precipitation trend for different spatial and temporal scales over Iran [29–38]. However, a few studies have investigated the historical trend and changes in extreme precipitation over Iran. The authors of [39] showed that there is a risk of extreme rainfall for at least 20% of the areas across Iran, according to observed data from 1982 to 2004. The investigation of extreme precipitation trends exhibited a strong positive trend in the daily precipitation from 1951 to 2007 over Iran [1].

There is an agreement that extreme precipitation events are increasing over time. It is generally expected that such increases translate to a general wetting feature. However, increasing the extreme precipitation may not always lead to an increase in the total precipitation. A decrease in moderate rainfall and an increase in the length of dry periods can offset the increased precipitation falling during heavy events. Global studies have indicated that extreme precipitation is increasing in a warming world, while the sensitivity of the annual precipitation to temperature showed significant variability due to the local climate during the last decades [40]. Due to the complexity of climate systems, spatiotemporal trends of precipitation features may be influenced by various regional and global phenomena, especially temperature warming. The earlier studies were focused on the assessment of historical variability and trends in extreme rainfall over time [41,42], while investigations on the sensitivity of extreme precipitation and annual precipitation to changes in temperature are generally lacking.

This study presented a comprehensive overview of the spatiotemporal changes in precipitation characteristics (maximum and annual precipitation) with increased temperature, as well as over time, contrasting the current literature to detect the historical variability and trends just over time. Eleven precipitation indices were analyzed to capture the changes in pattern and different characteristics of extreme rainfall. The present study advanced the previous extreme precipitation analysis [33,38,43–46] by employing the nonparametric Mann–Kendall test and the quantile regression (QR) methods to provide a more comprehensive picture of extreme precipitation events over Iran. The QR method helps us detect the plausible trends in probability distribution and different (especially upper) quantiles of the observed time series. Toward this end, sub-daily data from synoptic weather stations in Iran were used from 1951 to 2019. This study aimed to: (i) investigate the spatiotemporal trends in precipitation features (maximum and annual precipitation) and (ii) detect the sensitivity of the precipitation features (maximum and annual precipitation) to temperature warming.

2. Data and Methods

2.1. Data Description

The hourly precipitation records for the study 1951–2019 period (January 1951–December 2019) from 26 synoptic meteorological stations were obtained from the Meteorological Organization of Iran (Figure 1 and Table 1). The period for available precipitation data varied between 33 and 69 years from 1951 to 2019 for the selected stations (Figure 2). The selected stations are well-distributed across Iran and six main basins, including the Central Plateau Basin, the Persian Gulf and Oman Sea Basin, the Lake Urmia Basin, the Caspian Sea Basin, the Eastern Border Basin, and the Qareqom Basin (Figure 1). Generally, Northern and Western Iran indicate the maximum annual precipitation, and Central and Eastern Iran experience the lowest annual precipitation over Iran. The annual average air temperature

increases by moving towards Central and Southern Iran, while the average air temperature decreases in the northern and western regions of Iran (Figure 1d).
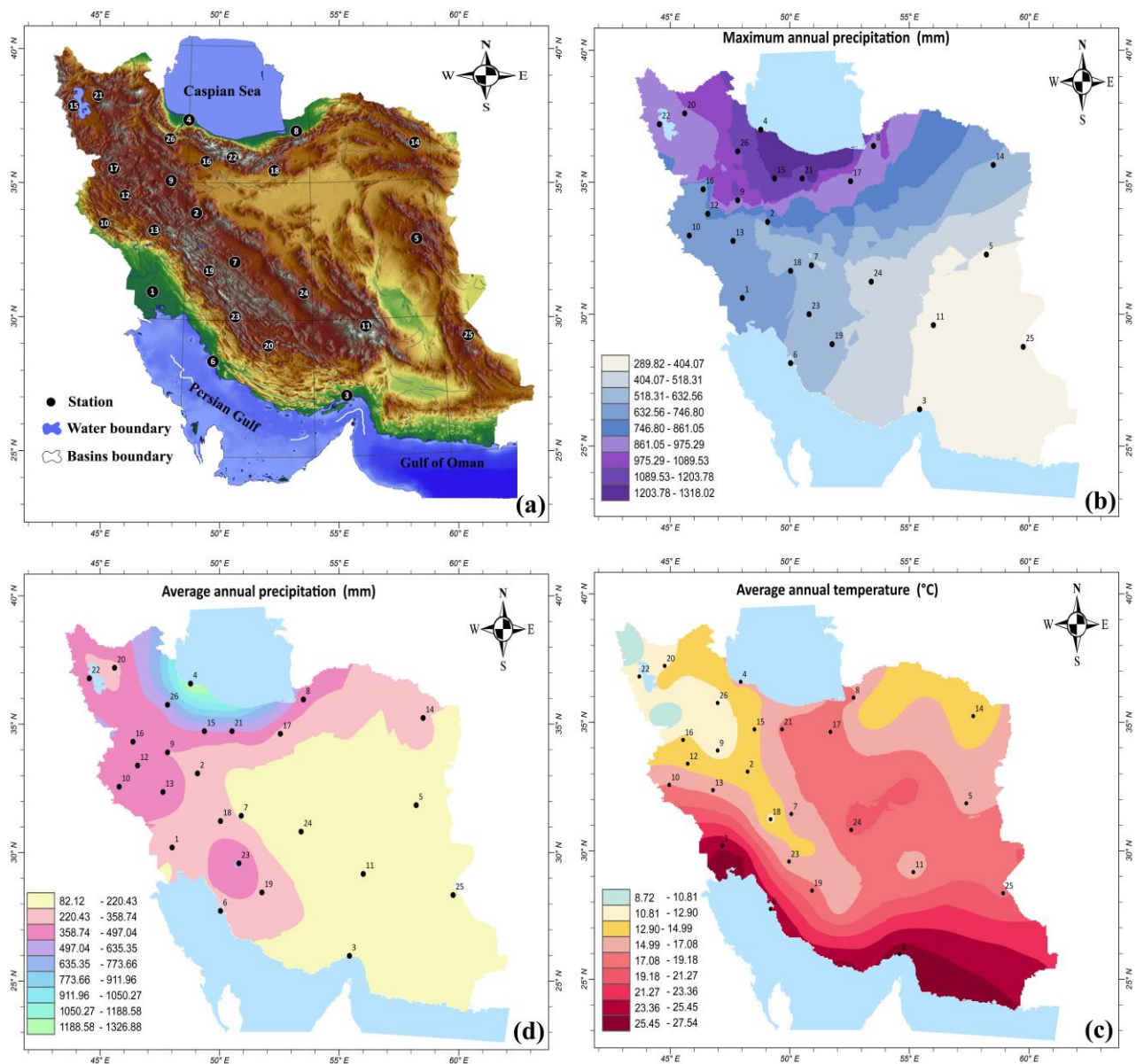
Figure 1. (**a**) Topographic map of Iran and the geographical locations of the selected stations, and spatial distributions of (**b**) the maximum annual precipitation, (**c**) average annual precipitation, and (**d**) average annual air temperature over Iran.

Table 1. Geographical characteristics and location of the selected stations.

No.	Station	Longitude (E)	Latitude (N)	Altitude (m)	River Basin
1	Ahvaz	48.7	31.3	22.5	Persian Gulf and Oman Sea
2	Arak	49.8	34.1	1702.8	Central Plateau
3	Bandar Abbas	56.4	27.2	9.8	Persian Gulf and Oman Sea
4	Bandar Anzali	49.5	37.5	−23.6	Caspian Sea
5	Birjand	59.3	32.9	1491.0	Central Plateau
6	Bushehr	50.8	28.9	8.4	Persian Gulf and Oman Sea
7	Isfahan	51.7	32.5	1550.4	Central Plateau
8	Gorgan	54.4	36.9	0.0	Caspian Sea
9	Hamedan	48.5	34.9	1740.8	Central Plateau
10	Ilam	46.4	33.6	1337.0	Persian Gulf and Oman Sea
11	Kerman	57.0	30.3	1754.0	Central Plateau
12	Kermanshah	47.2	34.4	1318.5	Persian Gulf and Oman Sea
13	Khorramabad	48.3	33.4	1147.8	Persian Gulf and Oman Sea
14	Mashhad	59.6	36.2	999.2	Qareqom
15	Urmia	45.1	37.7	1328.0	Lake Urmia
16	Qazvin	50.1	35.7	1279.1	Central Plateau
17	Sanandaj	47.0	35.3	1373.4	Persian Gulf and Oman Sea
18	Semnan	53.4	35.6	1127.0	Central Plateau
19	Shahrekord	50.8	32.3	2048.9	Persian Gulf and Oman Sea
20	Shiraz	52.6	29.6	1488.0	Central Plateau
21	Tabriz	46.2	38.1	1361.0	Lake Urmia
22	Tehran	51.3	35.7	1191.0	Central Plateau
23	Yasuj	51.6	30.7	1816.3	Persian Gulf and Oman Sea
24	Yazd	54.3	31.9	1230.2	Central Plateau
25	Zahedan	60.9	29.5	1370.0	Eastern Border
26	Zanjan	48.5	36.7	1659.4	Caspian Sea
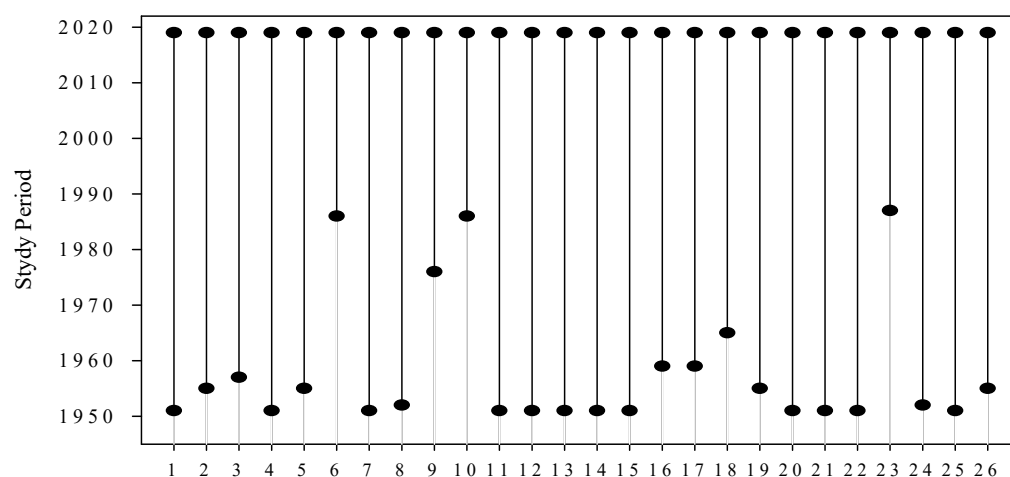
Figure 2. Study period of the precipitation and air temperature data at each station.

2.2. Extreme Precipitation and Air Temperature Indices

In this study, 14 different indices were employed to study the patterns of extreme rainfall and air temperature over Iran (Table 2). These indices were applied to analyze the trend of precipitation (Indices 1–11) and analyze the trend of temperature (Indices 12–14) over time, as well as under increased air temperature (Indices 1, 3, and 10), over the selected stations.

Table 2. The extreme rainfall indices and air temperature indices used for the trend analysis and their definitions.

Indices	Definition	Unit
Index 1	The maximum 3-h precipitation	mm
Index 2	The maximum 6-h precipitation	mm
Index 3	The maximum 24-h precipitation	mm
Index 4	The average 3-h precipitation	mm
Index 5	The average 6-h precipitation	mm
Index 6	The average 24-h precipitation	mm
Index 7	The number of 3-h precipitation above 95% quantile	number
Index 8	The average of extreme 3-h precipitation	mm
Index 9	The ratio of the 3-h extreme precipitation to annual precipitation	%
Index 10	The annual precipitation	mm
Index 11	The number of wet days	days
Index 12	The average annual temperature	°C
Index 13	The maximum annual temperature	°C
Index 14	The minimum annual temperature	°C

2.3. Trend Analysis

In this study, the Mann-Kendall test and quantile regression method were applied to detect the spatiotemporal trends in the defined extreme rainfall indices and air temperature indices over Iran.

2.3.1. Mann-Kendall Test

The Mann–Kendall (MK) test is a rank-based nonparametric test for detecting a monotonic trend in a time series. The method was originally proposed by [47], and the test–statistic distribution was subsequently derived by [48]. Since the distributions of most hydrometeorological data are skewed, it is appropriate to use a nonparametric test such as the Mann–Kendall test. In this study, we used the Mann–Kendall test to detect the trends of extreme precipitation indices, as the test is more attractive and more powerful than ordinary parametric trend tests for non-normally distributed series [49].

The Mann–Kendall test statistics (S) are computed as:

$$S = \sum_{i=1}^{N-1} \sum_{j=i+1}^{N} \text{sgn} \, (x_j - x_i) \tag{1}$$

where n is the number of data points, x_i and x_j are the data values in time series i and j (j > i), respectively, and sgn $(x_j - x_i)$ as the sign function is defined as:

$$\text{sgn} \, (\theta) = \text{sgn} \; (x_j - x_i) = \left\{ \begin{array}{cc} -1 & \theta < 0 \\ 0 & \theta = 0 \\ 1 & \theta > 0 \end{array} \right\} \tag{2}$$

If $n > 10$, the variance is computed as:

$$Var(s) = \frac{n(n-1)(2n+5) - \sum_{i=1}^{P} t_i(t_i - 1)(2t_i + 5)}{18} \tag{3}$$

Else, if $n \leq 10$, the variance is computed as:

$$\text{var}(s) = \frac{n(n-1)(2n+5)}{18} \tag{4}$$

where P is the number of tied groups, the summary sign ($\sum$) denotes the summation over all tied groups and the number of data in the ith (tied) group. If the tied groups are not

available, this summation process is excluded from the equation. Then, the standard Z value of the test statistics can be calculated as:

$$Z = \begin{cases} \dfrac{S-1}{\sqrt{\text{var}(s)}} & S > 0 \\ 0 & S = 0 \\ \dfrac{S+1}{\sqrt{\text{var}(s)}} & S < 0 \end{cases} \tag{5}$$

Positive values of Z indicate increasing trends, while negative Z values show decreasing trends. Testing trends are performed at a specific α significance level. When $|Z| > Z_{1-\alpha/2}$, the null hypothesis is rejected, and a significant trend exists in the time series. $Z_{1-\alpha/2}$ is obtained from the standard normal distribution table. In this study, a significance level $\alpha = 0.05$ was used. The null hypothesis of no trend is rejected if $|Z| > 1.96$ at the 5% significance level.

Reference [50] suggested a pre-whitening of the time series to eliminate the influence of a serial correlation on the Mann–Kendall test. Possible statistically significant trends in the sample data ($x_1, x_2, \ldots, x_n$) are examined using the following procedures:

Step 1: Compute the lag-1 serial correlation coefficient (r_1). The lag-1 serial correlation coefficient of the sample data x_i can be computed as [51]:

$$r_1 = \frac{\dfrac{1}{n-1} \sum\limits_{i=1}^{n-1} (x_i - \bar{x})(x_{i+1} - \bar{x})}{\dfrac{1}{n} \sum\limits_{i=1}^{n} (x_i - \bar{x})^2} \tag{6}$$

where $\bar{x}$ is the mean of the sample data, and n is the sample size.

Step 2-1: If the calculated r_1 is true in Equation (7) at $\alpha = 0.05$, the Mann–Kendall test can be used.

$$\frac{-1 - Z(1 - \frac{\alpha}{2})\sqrt{n-2}}{n-1} \le r_1 \le \frac{-1 + Z(1 - \frac{\alpha}{2})\sqrt{n-2}}{n-1} \tag{7}$$

Step 2-2: If the calculated r_1 is false in Equation (7), the data has a serial correlation that must be corrected as follows:

First, Sen's nonparametric trend estimator [52] is calculated as:

$$\beta = Median\left(\frac{x_j - x_l}{j - l}\right) \tag{8}$$

where x_i and x_j are the data values at times j and k (j > k), respectively.

Then, the value of y_i is calculated by using Equations (9)–(11):

$$x'_i = x_i - (\beta * i) \tag{9}$$

$$y'_i = x'_i - r_1(x'_{i-1}) \qquad y'_1 = x'_1 \tag{10}$$

$$y_i = y'_i + (\beta * i) \tag{11}$$

Finally, the trend of y_i is calculated by Equations (1)–(5).

2.3.2. Correlation Analysis

In this study, the Pearson's correlation coefficient was used to examine the correlation between the extreme precipitation indices (X) and the latitude, longitude, and latitude of each station (Y):

$$r = \frac{\sum (x_i - \bar{x})(y_i - \bar{y})}{\sqrt{\sum (x_i - \bar{x})^2 \sum (y_i - \bar{y})^2}} \tag{12}$$

where $\bar{x}$ and $\bar{y}$ are the mean values of x and y, respectively. The statistical significance for the correlation coefficient was calculated using the Student's *t*-test at the 5% significance level.

2.3.3. Quantile Regression

The quantile regression model can be defined by stating the traditional linear regression model as Equation (13):

$$y = a + bx + \varepsilon \tag{13}$$

where y and x are dependent and independent variables, respectively; a and b are regression coefficients representing the intercept and linear slope, respectively; and ε is the random error term associated with the regression. Within the classical linear regression framework, the regression coefficients (a and b) are estimated by the method of least squares. Considering n pairs of observed data x_i and x_j, this method minimizes the sum of squared errors, i.e.,

$$\min \sum_{i=1}^{n} (y_i - a - bx_i)^2 \tag{14}$$

The obtained $y'_i = a' + b'x_i$, where a' and b' denoted the estimated coefficients, is the conditional mean of a given x_i. If the regression coefficients a and b are estimated by minimizing the sum of absolute deviations, which is given by Equation (15):

$$\min \sum_{i=1}^{n} |y_i - a - bx_i| \tag{15}$$

the obtained y'_i then becomes the conditional median. Equation (15) is a special case of the quantile regression with 0.5 quantiles. The linear quantile regression model is the analogy to Equation (13), except that the regression coefficients are quantile-dependent. That is,

$$y_q = a_q + b_q x + \varepsilon_q \tag{16}$$

where q is a quantile ranging between 0 and 1, and a_q and b_q are regression coefficients that depend on the selected quantile (q) estimated by Equation (17) (minimizing the sum of asymmetrically weighted absolute deviations):

$$\min \sum_{i: \; y_i \geq a_q + b_q x_i} q|y_i - a_q - b_q x_i| + \sum_{i: \; y_i < a_q + b_q x_i} (1-q)|y_i - a_q - b_q x_i| \tag{17}$$

In this study, y denotes the rainfall indices, and x is the year of record or corresponding temperature. Dissimilar to the linear regression model, the regression coefficients of linear quantile regression (a_q and b_q) in Equation (16) cannot be found analytically. The slope b_q significantly different from zero is an indication of a linear trend at the qth quantile of a rainfall index when the corresponding p-value is less than 0.05 [53].

The QR method was applied here to investigate the temporal trend in different quantiles of the historical time series of Indices 1–11. This method was also used to detect the sensitivity of extreme precipitation (Indices 1 and 3) and annual precipitation (Index 10) in different percentiles to temperature warming.

3. Results and Discussion

3.1. Spatiotemporal Precipitation Trend by the Mann–Kendall Test

According to Table 3 and Figure 3, The maximum 3-h and 6-h precipitations (Indices 1 and 2) exhibited a decreasing trend in all stations (15 statistically significant $p < 0.05$), except Isfahan and Gorgan. There was a clear upward trend in the annual maximum 24-h precipitation for 10 stations, including Kermanshah ($p > 0.05$), Khorramabad ($p < 0.05$), Yasuj ($p > 0.05$), Isfahan ($p > 0.05$), Hamadan ($p > 0.05$), Qazvin ($p > 0.05$), Semnan ($p > 0.05$), Tehran ($p > 0.05$), Urmia ($p > 0.05$), and Gorgan ($p < 0.05$) Stations; this tendency was more

accentuated in Western and Central Iran (Figure 3). These upward trends have increased the risk of flash flooding in Isfahan and Gorgan Stations, as well as the mentioned stations located in the Central Plateau Basins, which should be also known as the susceptible area to flash flooding in Iran. Likewise, other studies confirmed similar tendencies in 24-h precipitation over Western Iran and Isfahan, Qazvin, Semnan, Tehran, and Gorgan Stations [34,37]. The Gorgan Station results are consistent with [54], who reported that the maximum daily precipitation has an increasing trend, while [38,55] showed a negative trend at this station. Moreover, the research of [56] indicated an insignificant increasing trend in precipitation in Southwestern Iran.

At the other stations, a negative trend was recognized for the annual maximum 24-h precipitation (statistically significant at Kerman, Bandar Anzali, and Zahedan Stations), showing the lower levels of flash flood risk (Table 3). In this regard, our results are consistent with [38,57,58].

Figure 3 shows that the average 3-h precipitation (Index 4) and the average 6-h precipitation (Index 5) decreased within the study period for all stations in the Persian Gulf, the Central Plateau River, Urmia Lake, Caspian Sea, Eastern Border River, and Qareqom Basins.

Except for Isfahan and Hamedan, the 3-h precipitation above the 95% quantile (Index 7) followed a decreasing trend at most Northern and Western Iran stations, including Urmia Lake, Caspian Sea, and the Eastern Border River Basins (Figure 3). These negative trends were statistically significant ($p < 0.05$) at stations in the northern region of Iran, as well as at Arak, Kerman, Shiraz, and Zahedan Stations.

A decreasing trend was detected in the average of the extreme 3-h precipitation (Index 8) at 23 stations (13 stations statistically significant). Regarding this index, an increasing trend was observed for Isfahan and Gorgan Stations, indicating that these regions have the potential for flash floods. The ratio of the 3-h extreme precipitation to annual precipitation (Index 9) had a decreasing trend at 25 stations (18 stations with a statistically significant ($p < 0.05$) trend), while Hamedan Station experienced a statistically insignificant ($p > 0.05$) increasing trend.

The decreasing trends in the annual precipitation (Index 10) were observed at 19 stations (5 stations with a statistically significant $p < 0.05$ trend). The annual precipitation increased during the study period at Kermanshah, Shahrekord, Isfahan, Hamedan, Qazvin, and Tehran Stations. However, Index 10 has a significant negative ($p < 0.05$) trend in Sanandaj, Kerman, Tabriz, Gorgan, and Zahedan Stations.

These results of the total annual precipitation are concomitant with the studies by [59–61], which reported a decreasing trend in Western and Northwestern Iran. The authors of [38] also reported a decreasing trend in precipitation in 60% of stations located in Western Iran during the 1966–2005 period.

The results showed a decreasing trend in the total annual precipitation of Bandar Abbas, Khorramabad, Sanandaj, Arak, Birjand, Semnan, Shiraz, and Yazd and the stations located at Urmia Lake and the Caspian Sea, as well as the Eastern Border Basins, while the number of rainy days had an increasing trend, which showed the occurrence of lighter rainfall in these regions. Our results are consistent with [61], who reported that the precipitation indices have a decreasing trend in the majority of the stations over Iran. Generally, the results indicated that it is plausible for flooding even in areas where drier conditions and decreasing annual rainfall trends have been experienced during recent decades, which agrees with [62]. The increasing trend in the number of rainy days (Index 11) was detected at 20 stations (10 stations with statistically significant ($p < 0.05$) trends). However, six stations showed decreasing trends (two stations with significant ($p < 0.05$) trends) in Index 11. Generally, the western stations showed a steeper trend slope in Index 11. According to [59–61], Northwestern and Western Iran showed a sharply decreasing trend in the wet days' index (Index 11), which complied with our results. The annual precipitation experienced an increasing trend at Isfahan and Qazvin Stations, while the number of rainy days had a decreasing trend, leading to the high risk of heavy rainfall at these stations.
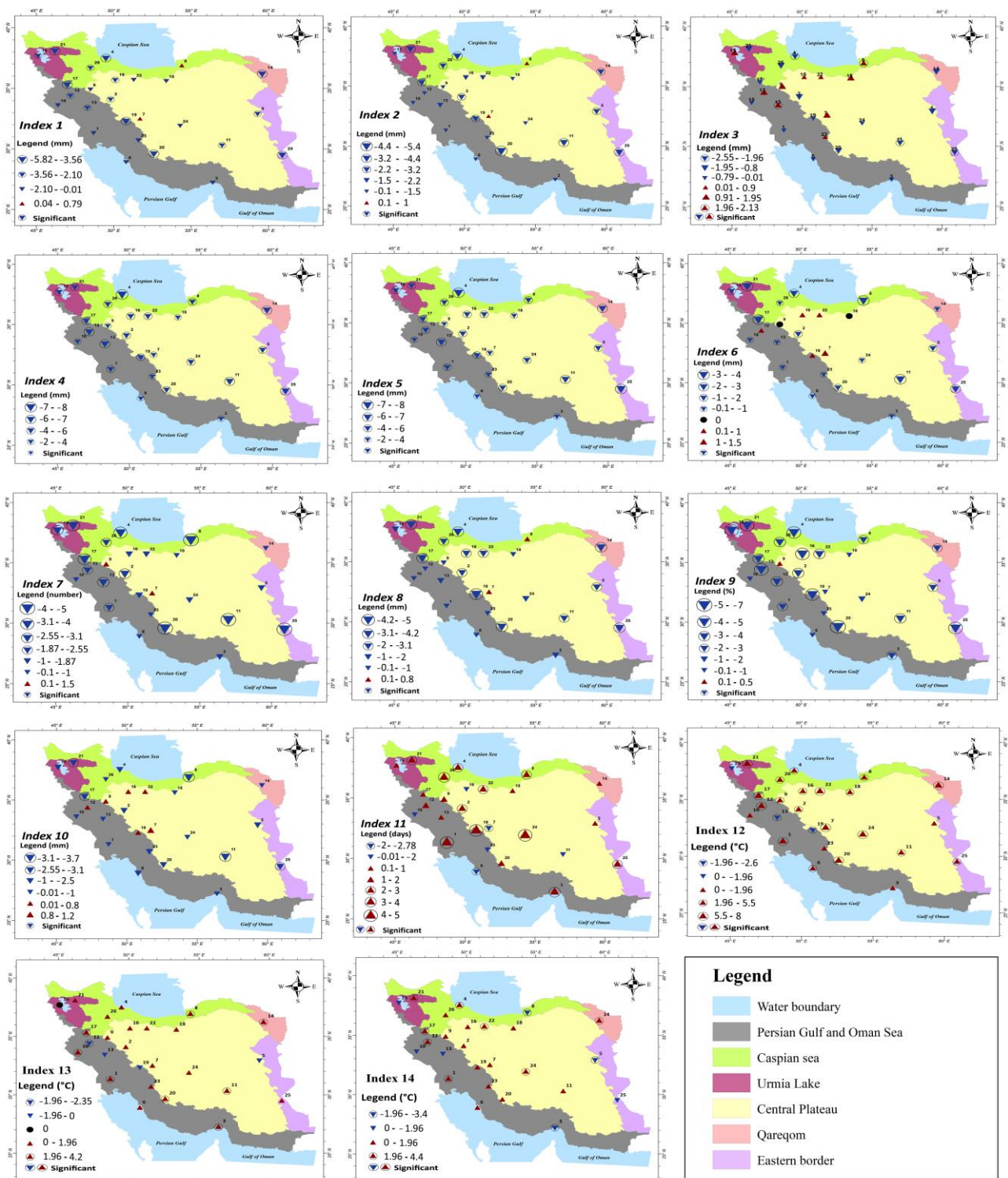
Figure 3. Spatiotemporal trend of the selected extreme precipitation and air temperature indices over Iran.

Table 3. Results of the Mann–Kendall test for the studied extreme rainfall indices. Blue and red numbers denote those statistically significant at the 0.05 critical level downward and upward trends.

Basin	Stations	Index 1	Index 2	Index 3	Index 4	Index 5	Index 6	Index 7	Index 8	Index 9	Index 10	Index 11
The Persian Gulf and Oman Sea	Ahvaz	−1.163	−0.86	−0.178	−5.63	−5.64	−0.664	−2.46	−0.326	−2.82	−0.628	4.397
	Bandar Abas	−1.531	−1.44	−0.419	−3.67	−3.67	−0.616	−1.855	−1.383	−2.399	−0.627	3.857
	Bushehr	−0.666	−1.28	−0.387	−2.81	−2.81	−0.563	−0.899	−0.418	−0.697	−1.224	−2.616
	Ilam	−0.847	−1.32	−0.565	−2.31	−2.31	−0.830	−0.328	−0.771	−0.415	−0.474	−1.202
	Kermanshah	−2.181	−1.2	1.27	−6.01	−6.01	0.108	−1.977	−0.927	−4.42	0.025	1.425
	Khorramabad	−2.458	−1.67	2.048	−6.34	−6.34	−0.927	−2.735	−1.466	−3.636	−0.751	0.098
	Sanandaj	−4.394	−3.1	−0.361	−6	−6	−3.310	−3.419	−4.108	−3.989	−2.889	0.641
	Shahrekord	−4.235	−2.4	−0.476	−5.15	−5.16	0.549	−1.591	−4.942	−5.023	0.753	4.438
	Yasuj	−1.195	−0.76	0.387	−2.09	−2.06	−0.852	−0.265	−0.418	−0.232	−1.348	−0.637
Central Plateau	Arak	−3.503	−3.1	−1.140	−5.55	−5.08	−1.636	−2.847	−2.923	−3.702	−1.285	2.634
	Birjand	−3.083	−2.3	−1.411	−5.28	−5.23	−1.111	−1.796	−2.37	−2.689	−1.058	0.799
	Isfahan	0.312	0.74	1.892	−3.71	−3.71	1.31	0.561	0.355	−0.338	1.11	−2.78
	Hamedan	−1.455	−1.32	1.275	−3.26	−3.26	0	1.313	−0.233	0.355	0.354	1.144
	Kerman	−2.478	−3.4	−2.095	−6.96	−6.95	−3.361	−4.208	−2.964	−3.762	−3.289	−0.845
	Qazvin	−2.414	−1.92	0.666	−5.08	−5.07	0.653	−1.063	−2.453	−4.188	0.777	−0.473
	Semnan	−0.0874	−0.26	1.82	−3.62	−3.61	0	−0.118	−0.705	−0.508	−0.716	0.029
	Shiraz	−5.822	−5.1	−1.583	−5.70	−5.70	−1.253	−4.023	−3.773	−6.442	−1.273	1.861
	Tehran	−1.504	−1.73	0.658	−5.24	−5.25	0.419	−1.796	−2.14	−3.299	0.57	2.176
	Yazd	−1.444	−1.37	−0.349	−4.06	−4.06	−0.397	−1.107	−1.49	−1.906	−0.153	4.723
Urmia Lake	Urmia	−2.138	−0.99	1.135	−5.75	−5.57	−1.238	−3.053	−1.575	−4.822	−1.212	0.466
	Tabriz	−4.108	−3.4	−1.705	−5.79	−5.78	−3.308	−3.605	−3.5	−4.113	−2.543	2.436
Caspian sea	Bandar Anzali	−3.926	−3.7	−2.160	−7.25	−7.26	−2.056	−3.828	−4.133	−5.023	−1.818	2.529
	Gorgan	0.556	0.86	2.123	−5.48	−5.48	−3.431	−4.097	0.606	−2.478	−3.701	2.982
	Zanjan	−2.763	−2.9	−0.912	−5.57	−5.57	−0.888	−2.540	−2.69	−3.572	−0.379	3.885
Eastern border	Zahedan	−3.789	−3.6	−2.551	−7	−7	−2.989	−4.716	−3.64	−4.784	−2.853	2.805
Qareqom	Mashhad	−3.925	−2.7	−0.886	−6.34	−6.34	−0.16	−0.90	−3.73	−2.988	−0.16	0.819

3.2. Spatiotemporal Air Temperature Trend by Mann-Kendall Test

The average air temperature (Index 12) exhibited an increasing trend in all stations (19 statistically significant $p < 0.05$), except Khorramabad, Shahrekord, and Urmia. The decreasing trends in the maximum annual temperature (Index 13) were observed at Birjand, Kermanshah, Khorramabad, and Shahrekord Stations, while only Kermanshah Station indicated a statistically significant trend. The annual minimum temperature (Index 14) had a positive trend in all stations (eight stations with a statistically significant ($p < 0.05$) trend), except Bandar Abbas, Birjand, Gorgan, Ilam, Khorramabad, Urmia, and Zahedan Stations. Generally, the stations located in the central, northern, and southern regions of Iran face an increase in temperature, while this trend was reversed in Western and Northwestern Iran.

Our results are consistent with [63,64], who reported increasing tendencies of the temperature in the majority of the stations over Iran.

3.3. Maximum Daily Precipitation Analysis

The annual maximum 24-h precipitation series showed an increasing tendency in Western and Central Iran, while there was no general pattern over Iran. The IPCC report confirmed that extreme precipitation differs from annual precipitation due to considerable geographical differences in events' frequency, timing, and magnitude [65].

In Western Iran (Isfahan, Yasuj, Hamedan, and Kermanshah Stations), annual the maximum 24-h precipitation was more frequent during March, November, and February (Figure 4). However, the annual maximum 24-h precipitation was in Central Iran (Tehran, Qazvin, and Semnan Stations).

Precipitation occurs mainly during February and March. At Gorgan and Urmia Stations, the annual maximum 24-h precipitation had the most frequency during November and April, respectively. However, there is no single dominant season, and the occurrence of an extreme event can arrive at any time of the year at Hamedan Station. The recent peaks of the annual maximum 24-h precipitation of Gorgan, Kermanshah, Khorramabad, and Yasuj Stations mainly occur in March. Increasing the elevation means annual maximum 24-h precipitation occurs from the fall season (November) to the winter season (February and March).

In agreement with similar studies over the globe, our investigation revealed that the annual maximum daily precipitation trend over Iran is complex. For example, the upward trends in extreme precipitation were detected in the USA, China, Australia, Canada, Norway, Mexico, and Poland [66], where no clear trend was experienced in the regions such as Brazil and Ethiopia [67,68].

3.4. Quantile Regression Results

3.4.1. Temporal Precipitation Trend Analysis

Quantile regression was here applied to study the temporal change in the defined indices based on the different quantiles for the data distribution. The slopes of the 10th, 25th, 50th, 75th, and 90th quantile regression lines have been estimated for the indices to investigate the trends and changes in extreme rainfall over Iran (Table 4).

The maximum 3-h precipitation (Index 1) exhibited a decreasing trend at 24 out of 26 stations (13 statistically significant trends ($p < 0.05$)), and two stations showed an increasing trend ($p > 0.05$) for the slope of the 50th quantile regression line, while the Mann–Kendall method had a decreasing trend at 24 out of 26 stations (15 statistically significant ($p < 0.05$) trends). The maximum 6-h precipitation (Index 2) exhibited a decreasing trend at 17 stations (two statistically significant trends ($p < 0.05$)), while 7 stations showed an increasing trend (one statistically significant trend ($p < 0.05$)) for the slope of the 25th quantile regression line, which was inconsistent with the results of the Mann–Kendall test.
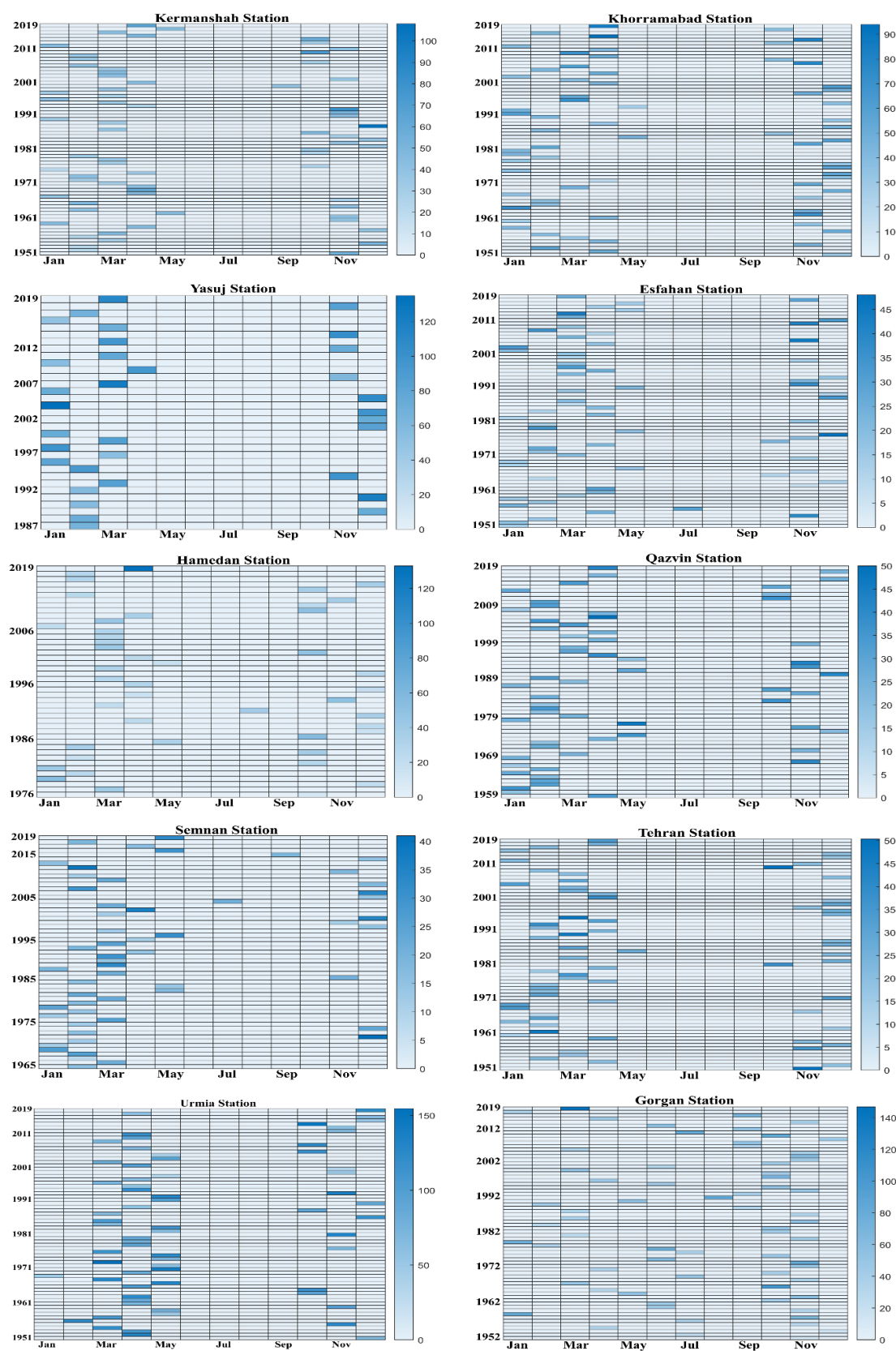
Figure 4. Heat map of the timing and depth of the annual maximum daily precipitation.

Table 4. The quantile regression coefficients for selected percentiles ($\times 10^{-2}$). Blue and red numbers denote statistical significance at the 0.05 critical level downward and upwards trends.

Stations	Index 1					Index 2					Index 3					Index 4				
Quantile Re.	0.1	0.25	0.5	0.75	0.9	0.1	0.25	0.5	0.75	0.9	0.1	0.25	0.5	0.75	0.9	0.1	0.25	0.5	0.75	0.9
Ahvaz	−10.53	−5.41	−6.45	−25.81	−13.04	−15.56	−3.92	0	−27.86	−20.91	−6.67	0	0	−25	11.4	−0.18	−0.16	−0.35	−0.48	−0.67
Bandar Abas	0.71	−7.69	−12.5	−32	11.11	−5.26	−10.53	−25	−22.4	27.78	1.05	−4.35	−11.11	−4.35	55.5	−0.11	−0.21	−0.26	−0.37	−0.34
Bushehr	−44.44	−46.15	−27.59	−132	−46.15	1.04	−34.78	−40.4	−21.7	−93.5	−18.52	1.75	2.44	−50.56	−105	−0.44	−0.4	−0.45	−0.76	0.03
Ilam	−18.18	−20	−8.27	−0.33	2.77	−15	−18.52	−42.1	2.82	175	−56.67	−41.18	0	95	74.5	−0.54	−0.53	−0.67	−0.6	−0.78
Kermanshah	−5.26	0	−16.67	−18.42	−13.21	−9.37	2.94	−22.7	−18.2	−16	14.81	16.38	3.18	0	9.34	−0.3	−0.28	−0.44	−0.88	−1.19
Khorramabad	−3.45	−12.12	−15.63	−17.19	11	−10	−18.64	−13.5	−8.75	11.9	8.33	7.31	3.92	27.27	49.2	−0.54	−0.56	−0.71	−1.04	−1.04
Sanandaj	−13.64	−25	−26.1	−30.6	−37.5	1.06	−27.5	−23	−23.2	−23.5	0.04	−6.37	−7.35	−2.56	17.3	−0.3	−0.64	−0.9	−1.18	−0.11
Shahrekord	−5.56	−9.09	−19.1	−27.3	−34.04	−12.2	−13.64	−17.8	−26.3	−22.9	−1.14	0.62	−9.26	2.22	2.82	−0.19	−0.29	−0.38	−0.59	−0.74
Yasuj	−14.29	−26.3	−21.05	0	−29.03	−16	−20	−37.5	−6.86	16.13	−10	3.47	4.16	5.11	5.5	−0.73	−1.01	−0.87	−0.4	−0.67
Arak	−5.26	−22.7	−24.39	−34.4	−30.15	23.02	14.63	−19.1	−24.4	−38.6	−18.75	−18.9	−7.41	6.67	−5.08	−0.3	−0.49	−0.53	−0.84	−0.73
Birjand	−4	−6.9	−15.4	−13.89	−22.22	−6.52	−7.69	−10.8	1.21	−22.2	−5.82	−7.89	−7.41	16.67	−11.4	−0.8	−0.22	−0.3	−0.36	−0.39
Esfahan	6.25	0	2.99	−3.45	−0.22	2	3.57	4.35	5.56	−5.56	7.27	3.92	16.13	13.56	22.4	−0.06	−0.07	−0.16	−0.24	−0.24
Hamedan	2.9	6.67	−0.17	−4.55	1.66	29.09	13.58	−3.45	−25	2.01	26.2	1.39	16.8	−2.78	5.88	0	−0.04	−0.35	−0.67	−0.41
Kerman	−4.55	−4.44	−6.67	−15	−16.67	0	−11.11	−19	−26	−27	−1.58	−3.7	−10	−18.72	−15	−0.09	−0.25	−0.29	−0.35	−0.4
Qazvin	0.65	−4	−11.11	−14.29	−14.81	−4.88	−3.48	−6.67	−15	−20	10.45	5.45	7.14	0.03	8.62	−0.23	−0.23	−0.46	−0.51	−0.6
Semnan	3.7	0	−2.44	−10	5.56	5	4.35	2.42	3.57	6.38	3.23	9.55	0	14.32	18.9	−0.12	−0.09	−0.13	−0.32	−0.47
Shiraz	−17.9	−23.4	−33.3	−46.8	−47.3	−14.58	−25	−41	−74	−100	1.91	−14.31	−9.14	−29.55	−75	−0.32	−0.26	−0.51	−0.73	−1
Tehran	0	−2.44	−6.9	−6.45	−4.55	0	−1.03	−7.81	−24	−16	6.38	3.33	2.89	−5.38	0	−0.16	−0.21	−0.28	−0.39	−0.52
Yazd	−4	−4.17	−6.12	−7.69	−14.29	−3	−4.84	−4	−14	−12.7	2.08	−3.11	0.69	0	−11.2	−0.04	−0.06	−0.08	−0.14	−0.18
Urmia	0	−15.2	−9.09	−6.9	−10	−12.64	−7.27	0	−5.56	2	−4.28	−1.96	17.39	13.31	21.5	−0.49	−0.52	−0.57	−0.63	−0.59
Tabriz	−9.7	−11.1	−13.64	−16.3	−21.8	−12.12	−11.11	−14.7	−10.7	−16.2	−5.26	−12.94	−6.67	−5.16	12	−0.38	−0.47	−0.49	−0.56	−0.76
Bandar Anzali	−29.27	−31.29	−52.63	−145	−242	−27.78	−46.15	−96	−161	12.65	−11.86	−13.33	−19.57	−87.76	12.6	−1.99	−2.48	−2.72	−3.39	−4.59
Gorgan	4	3.57	2.63	8.7	3.39	27.27	8.33	8.16	2.63	2.94	25.93	22.11	26.67	27.27	18.1	−0.27	−0.67	−1.13	−1.32	−1.6
Zanjan	−9.52	7.69	−14.7	−13.04	−17.19	−4.65	−10.87	−16	−14.8	−24.5	−4.06	−8.78	−7.67	−17.4	−14.2	−0.25	−0.37	−0.54	−0.68	−0.78
Zahedan	−10.53	−13.3	−17.6	−20.41	−20.45	−10.87	−14	−26	−17.6	−13.4	−13.54	−13.33	−11.22	−16.64	−17.6	−0.13	−0.17	−0.18	−0.25	−0.25
Mashhad	−10.26	−13.1	−15	−16.7	−18.4	−10.26	−11.82	−12.7	−20	−22.4	0	−6.86	−3.17	−10.34	−8.33	−0.29	−0.21	−0.36	−0.39	−0.48

Table 4. *Cont.*

Stations	Index 5					Index 6					Index 7					Index 8				
Quantile Re.	0.1	0.25	0.5	0.75	0.9	0.1	0.25	0.5	0.75	0.9	0.1	0.25	0.5	0.75	0.9	0.1	0.25	0.5	0.75	0.9
Ahvaz	0.35	−0.31	−0.69	−0.97	−1.28	0.07	0.02	−0.09	−0.15	−0.21	−1.89	−3.85	−5.2	−2.38	0.25	−1.47	2.59	3.11	7.14	8.11
Bandar Abas	−0.21	−0.42	−0.52	−0.73	−0.67	−0.06	−0.27	−0.02	0.04	−0.27	0	−2.27	−2.13	−1.79	0	2.17	−3.1	−1.9	−13.77	3.12
Bushehr	−0.88	−0.8	−0.9	−1.53	0.07	−0.97	−0.44	0.04	−0.37	−0.2	−3.7	−7.14	−4.76	−0.12	0	−4.17	1.3	0.7	25.61	10.51
Ilam	−1.09	−1.06	−1.35	−0.12	−1.56	−0.91	−0.68	−1.04	−1.6	0.12	0	0.29	0	−7.14	−6.12	−1.98	−3.6	−0.69	1.27	1.66
Kermanshah	−0.62	−0.56	−0.88	−1.76	−2.39	0.31	0.24	−0.3	−0.5	−0.85	0	−2.04	−2.63	−6.9	−14	−1.15	−3.52	0.07	−0.7	−2.29
Khorramabad	−1.08	−1.13	−1.42	−2.09	−2.07	−0.06	−0.27	−0.32	−0.46	0.11	−5.6	−6.7	−4.76	−5.13	−5.71	−7.1	−3.45	−3.19	0.81	−1.69
Sanandaj	−0.61	−1.28	−0.18	−2.36	−0.22	0.13	−0.57	−0.57	−1.23	−0.99	0	−9.7	−11	−15	−12.5	−6.8	−7.4	−8.3	−8.9	−12
Shahrekord	−0.39	−0.59	−0.76	−1.18	−1.48	0.13	0.16	0.16	−0.02	−0.09	0	0	−3.77	−8.34	−6.67	−3.49	−7.7	−9.3	−12	−15
Yasuj	−1.46	−2.02	−1.74	−0.81	−1.35	−1.56	−2.12	−0.16	−0.66	0.17	−5.88	−10	0	0	1.49	3.06	−3.57	−1.96	−4.48	−14.25
Arak	−0.59	−0.99	−1.07	−1.68	−1.47	−0.05	0.21	0.38	−0.09	−0.18	−4.17	−4.98	−6.67	−5.77	−9.84	−3.75	−4.02	−6.43	−9.6	−5.98
Birjand	−0.15	−0.43	−0.59	−0.72	−0.78	−0.07	−0.05	−0.01	−0.01	−0.22	0	−1.69	−2.86	−5.13	−5.08	−2.19	−3.03	−2.79	−5.72	−4.04
Esfahan	−0.12	−0.13	−0.3	−0.48	−0.48	0.15	0.15	0.07	0.13	0.08	1.92	0	0	1.75	0	1.15	0	0	−1.75	−2.98
Hamedan	0	−0.08	−0.7	−1.35	−0.82	0.32	−0.15	−0.25	−0.62	0.43	6.25	11.5	5.56	7.69	0.55	5	1.02	−2.69	−6.67	−7.5
Kerman	−0.18	−0.5	−0.58	−0.7	−0.8	−0.22	−0.2	−0.24	−0.32	−0.43	−2.04	−5.2	−4.7	−5.7	−11	−0.89	−1.19	−1.11	−2.27	−2.73
Qazvin	−0.46	−0.47	−0.92	−1.02	−1.2	0.21	0.4	0.02	−0.08	−0.5	−2.86	0	−8.33	−3.23	−14.63	−2.31	−5.1	−2.66	−0.38	2.38
Semnan	−0.24	−0.17	−0.27	−0.64	−0.93	0.01	0.11	−0.03	−0.06	−0.34	1.96	0	2.27	−3.33	−4.17	0.67	−1.73	0.99	−5	−3.74
Shiraz	−0.65	−0.52	−1.02	−1.45	−2	−0.48	0.16	−0.3	−0.4	−1.36	−4.3	−4.08	−6.7	−7.1	−16	−7.5	−6.5	−11	−14	−22.7
Tehran	−0.32	−0.41	−0.56	−0.78	−1.05	0.1	0.06	0.07	0.1	−0.31	−1.72	0	−4.62	−7.84	−9.6	−1.27	−2.47	−2.28	−1.78	−4.62
Yazd	−0.08	−0.13	−0.17	−0.28	−0.36	0.01	−0.02	0	−0.05	0.1	0	−1.72	0	−2.7	0	−1.48	−2.04	−2.54	−3.95	3.7
Urmia	−0.99	−1.04	−1.15	−1.27	−1.19	−0.34	−0.09	−0.39	−0.3	0.1	−10	−9.1	−8.7	−8	−3.28	−2.31	−5.1	−2.66	−0.38	2.38
Tabriz	−0.76	−0.95	−0.97	−1.12	−1.53	−0.27	−0.25	−0.33	−0.29	−0.62	−5.6	−7.1	−7.27	−5.71	−12.1	−1.8	−2.97	−2.56	−3.99	−3.09
Bandar Anzali	−3.97	−4.95	−5.44	−6.78	−9.19	−0.07	−0.05	−0.19	−0.01	−0.22	−5.26	−8.51	−19	−14.3	−15.22	−10	−12	−14	−28	−27
Gorgan	−0.54	−1.34	−2.26	−2.63	−0.32	−0.23	−0.76	−0.48	−0.82	−1.12	0	−8.33	−11	−12	−15.6	2.52	1.68	4.2	−1.65	0.36
Zanjan	−0.5	−0.73	−1.07	−1.37	−1.55	0.07	0.06	−0.07	−0.2	−0.51	−5.13	−5.41	−4.76	−9.76	−14.3	−2.5	−3.11	−4	−2.59	−3.49
Zahedan	−0.27	−0.34	−0.36	−0.51	−0.51	−0.14	−0.21	−0.2	−0.14	−0.31	−4.1	−4.1	−4.5	−5.4	−3.4	−2.08	−1.6	−4.78	−6.41	−6.67
Mashhad	−0.58	−0.42	−0.73	−0.78	−0.97	0	0.07	−0.12	−0.11	−0.17	−2.04	−3.23	−0.00	−1.52	−0.00	−3.51	−4.3	−4.3	−2.56	−5.45

Table 4. *Cont.*

| Stations	Index 9					Index 10					Index 11				
Quantile Re.	−0.3	−0.4	−0.4	−0.22	−0.4	5.23	−11.3	−5.53	−54.7	−61	32.69	50	34.9	38.5	25.1
Ahvaz	0	−0.7	−0.41	−0.29	−0.05	−21.2	−21.7	−6.69	4.02	−99.9	11.54	17.1	15.6	20	15.25
Bandar Abas	−0.68	−0.89	−0.45	0.14	0.38	−115	3.42	−18.8	−291	−719	−29.1	−23.1	−38	−33.3	−46.1
Bushehr	−0.04	0.21	−0.16	−0.02	−0.06	21.24	−246	30.07	429.3	41.52	−2.74	−44.4	−26.9	−81.5	−6.45
Ilam	−0.01	−0.2	−0.3	−0.24	−0.13	87.98	78.97	−134	−316	−437	31.82	10.81	4.55	24.53	20
Kermanshah	−0.3	−0.18	−0.3	−0.3	−0.25	16.88	5.53	−89.8	21.16	41.32	7.46	−1.69	14.29	−11.1	−4.55
Khorramabad	−0.19	−0.3	−0.5	−0.4	−0.5	13.92	−168	−195	−428	−160	17.5	10.53	12.5	0	2.94
Sanandaj	−0.12	−0.3	−0.4	−0.5	−0.6	45.58	81.34	47.83	−6	22.92	43.5	53.8	36.8	5	37.3
Shahrekord	−0.04	−0.24	−0.23	0.34	0.2	−392	30.6	42.12	−844	−619	36.84	0	−9.09	−40.9	−13.3
Yasuj	−0.5	−0.3	−0.4	−0.4	−0.41	9.84	−75.1	−15.1	−89.4	−188	32.5	31	36.4	4.35	27.27
Arak	−0.05	−0.3	−0.3	−0.5	−0.4	−26.7	−7.87	−54.3	−30.5	11.16	7.14	8.33	0	−5.45	−9.62
Birjand	0.23	0.08	−0.05	0.08	−0.14	50.51	48.29	26.05	28.89	34.04	−10.6	−7.41	−17	2.46	−42
Esfahan	0.4	0.32	0.15	−0.24	−0.15	10.07	12.84	−31.2	18.8	80.63	23.65	31.25	4.55	31.25	44.44
Hamedan	−0.27	−0.4	−0.3	−0.4	−0.5	−33.3	−74	−83.5	−90.3	−155	0	6.9	−8.7	−10.3	−29.7
Kerman	−0.17	−0.2	−0.3	−0.4	−0.4	78.21	13.07	58.9	14.84	−42	3.57	−22.7	0	−2.44	−11.1
Qazvin	0.07	−0.08	−0.03	−0.24	−0.19	20.3	39.51	−12.2	−23.2	11.65	0	−6.67	0	4.55	−15
Semnan	−0.6	−0.7	−0.5	−0.8	−0.7	−16.6	42.61	123.1	−144	−492	20.51	24.1	13.24	5.88	13.79
Shiraz	−0.05	−0.11	−0.4	−0.4	−0.3	39.57	39.82	25.32	33.33	−82.2	25.81	15.38	21.05	22.73	9.76
Tehran	0	−0.31	−0.5	−0.31	−0.09	5.88	20.76	−2.1	3.85	−29.9	30.6	34.7	29.3	27.27	18.42
Yazd	−0.4	−0.3	−0.3	−0.3	−0.05	−113	−36.6	−149	−110	36.56	20.83	6.67	12.24	3.47	−16.4
Urmia	−0.2	−0.3	−0.3	−0.2	−0.14	−97	−91.1	−127	−106	−161	34.1	39.2	13.79	18.87	22.5
Tabriz	−0.2	−0.3	−0.4	−0.5	−0.4	−21.2	−21.8	−606	−519	−128	18.18	24.07	34.8	27.8	59.3
Bandar Anzali	0.26	−0.11	−0.3	−0.16	−0.3	−84.2	−287	−176	−219	−38.4	7.14	31.82	47.2	35.1	6.44
Gorgan	−0.5	−0.5	−0.3	0.23	−0.4	30.23	34.48	−0.28	−92.4	−187	50.94	55.6	55.8	5	55.6
Zanjan	−0.8	−0.8	−0.7	−0.6	−0.6	1.58	−76.	−79	−70.2	−87.6	2.26	14.71	20.4	22.6	26.3
Zahedan	−0.37	−0.3	−0.2	−0.19	−0.3	3.97	24.43	−42.1	−41.5	17.36	23.5	3.54	4	4.44	−6.9
Mashhad	−0.3	−0.4	−0.4	−0.22	−0.4	5.23	−11.3	−5.53	−54.7	−61	32.69	50	34.9	38.5	25.1

There was an increasing trend in the maximum 24-h precipitation (Index 3) at Kermanshah, Khorramabad, Isfahan, Qazvin, Semnan, and Gorgan Stations in all quantile regression lines, indicating the possibility of flooding, which was similar to the results of the Mann–Kendall method. In all quantile regression lines, there was a decreasing trend in Index 3 at Kerman, Zanjan, Zahedan, and Mashhad Stations, and floods are unlikely. The average 3-h precipitation (Index 4) and the average 6-h precipitation (Index 5) exhibited a decreasing trend at most stations in the 50th and 75th quantiles, which was generally similar to the results of the Mann–Kendall method. The average 24-h precipitation (Index 6) had a decreasing trend at 14 stations (2 statistically significant ($p < 0.05$)), as well as an increasing trend at 10 stations on the slope of the 10th and 25th quantile regression lines, which were inconsistent with those of the Mann–Kendall method.

Similar to the Mann–Kendall test, there was no significant trend in the average 24-h precipitation (Index 6) of the stations located in the Persian Gulf and the Central Plateau River Basins, except Sanandaj and Kerman Stations, based on the 10th, 25th, 50th, and 75th quantiles. The amount of 3-h precipitation above the 95% quantile (Index 7) exhibited a decreasing trend at 18 out of 26 stations (10 statistically significant ($p < 0.05$)), and 3 stations showed an increasing trend (1 statistically significant ($p < 0.05$)) for the 25th quantile regression line.

The average of extreme 3-h precipitation (Index 8) followed a significant ($p < 0.05$) negative trend at Sanandaj, Shahrekord, Arak, Shiraz, Bandar Anzali, Zanjan, and Mashhad Stations, leading to a lower risk of a flash floods, which was consistent with the Mann–Kendall test. There was a decreasing trend in the annual precipitation (Index 10) in Kerman, Tabriz, Bandar Anzali, and Gorgan in all quantile regression lines, which was similar to the results of the Mann–Kendall method. The results showed an increasing trend in the number of wet days (Index 11) at 17 stations (8 stations with a statistically significant ($p < 0.05$) trend) and a decreasing trend for 5 stations (2 stations with statistically significant ($p < 0.05$) trends) in the slope of the 50th quantile regression line.

Generally, the results of the Mann–Kendall test had the highest and lowest consistency levels with the slopes of the 50th and 90th quantile regression lines results, respectively. The results of the Mann–Kendall method for Indices 1, 4, 5, and 9 were similar to the 50th percentile results of the quantile regression method (100% similarity). By using the Mann–Kendall and the quantile regression methods, the maximum 3-h precipitation (Index 1) and the maximum 6-h precipitation (Index 2) showed a decreasing trend at most stations, and these indicators were increasing at Gorgan and Isfahan Stations. Indicators 4 and 5 indicated a decreasing trend at the most stations by both methods. The average 24-h precipitation (Index 6) and the amount of 3-h precipitation above the 95% quantile (Index 7) exhibited an increasing trend at Isfahan Station. An increasing trend in Index 6 for Ahvaz, Isfahan, and Gorgan Stations revealed that these regions are at a high risk for flash floods. The annual precipitation increased during the study period at Shahrekord, Isfahan, Hamedan, Qazvin, and Tehran Stations, which showed the movement of these stations towards the wetter pattern in both methods. The total annual precipitation had an increasing trend at Isfahan and Qazvin Stations, while the number of rainy days had a decreasing tendency, which showed the high risk of heavy rain at these stations. The precipitation indices had a decreasing trend in the majority of the stations over Iran.

The estimated quantile regression lines could be used to detect plausible changes in the selected precipitation extremes indices over Iran. According to Figure 5, the quantile regression line for the percentile above 70% was ascending for the maximum 3-h and 6-h precipitations (Indices 1 and 2) at Gorgan Station. In accordance with the results of the Mann–Kendall method, there was a possibility of flash flooding at this station. At Kermanshah, Khorramabad, Isfahan, Hamedan, Qazvin, Semnan, and Urmia Stations, quantitative regression lines for percentiles above 70% (one-third of the data) were ascending for the maximum 3-h precipitation (Index 1). Therefore, these regions should be considered as susceptible areas to flash flooding.
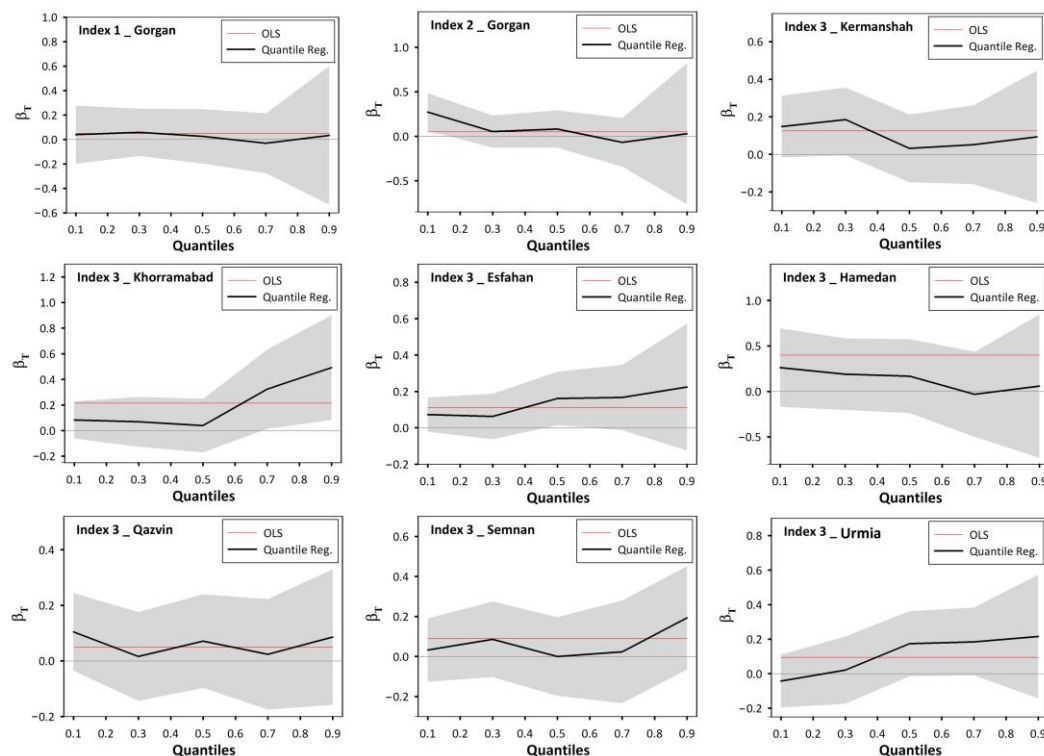
Figure 5. The quantile regression coefficients for extreme rainfall indices.

3.4.2. Precipitation Assessment with Increased Air Temperature

Quantile regression was used here to investigate whether the annual precipitation temperature sensitivity exhibited similar patterns as extreme precipitation temperature sensitivity over Iran (Table 5). The annual precipitation (Index 10) in all stations except Gorgan, Urmia, and Khorramabad Stations decreased under rising temperatures. We found that the maximum 3-h precipitation temperature sensitivity was positive throughout the analyses. In contrast, the annual precipitation temperature sensitivity was negative in Bandar Abbas; Sanandaj; Shahrekord; Urmia; Bandar Anzali; Gorgan; Ilam (90th quantile); Kermanshah (90th quantile); Isfahan (90th quantile); Zahedan (90th quantile); Hamedan (50th, 75th, and 90th quantiles); and Zanjan (75th and 90th quantiles), implying that, while the rising temperature has led to an increase in the incident precipitation, a decrease in the total was observed (Table 5). Our results indicated an increase in the 3-h precipitation at higher temperatures only in Ahvaz, Bushehr, Mashhad, Tabriz, Shiraz, Tehran, Kerman, and Qazvin (mostly located in arid Central Iran) corresponded to increases in the annual precipitation.

The results also indicated that the maximum 24-h precipitation temperature sensitivity was positive while the annual precipitation temperature sensitivity was negative in Bandar Abbas; Birjand; Sanandaj; Shahrekord; Isfahan; Qazvin; Urmia; Ilam (90th quantile); Kermanshah (90th quantile); Ahvaz (90th quantile); Khorramabad (90th quantile); Gorgan (10th, 25th, and 50th quantiles); and Hamedan (25th, 50th, and 75th quantiles), suggesting that the maximum precipitation in the daily time scale may not correspond to the annual precipitation. The lack of correspondence between the extreme precipitation and annual precipitation suggested that the sensitivity of extreme precipitation to temperature was not a good indicator of the interannual variability in annual precipitation in arid and semiarid regions, such as most parts of Iran. The only exception was for the stations such as Mashhad, Zanjan, Zahedan, Bushehr, and Kermanshah, where evidence of positive maximum precipitation and negative annual precipitation scaling was found only at the most extreme (90th) percentile.

Table 5. The quantile regression coefficients of the precipitation and temperature for the selected percentiles ($\times 10^{-2}$). Blue and red numbers denote statistical significance at the 0.05 critical level downward and upwards trends.

Stations	Index 1					Index 3					Index 10				
Quantile Re.	0.1	0.25	0.5	0.75	0.9	0.1	0.25	0.5	0.75	0.9	0.1	0.25	0.5	0.75	0.9
Ahvaz	−1.08	−0.833	−3.076	−0.625	−0.6	0.408	0.454	−1.42	−1.66	1.47	−5.01	−11.89	−14.10	−27.90	−28.66
Bandar Abas	1.57	2.173	1	4.7	3.84	3.71	2.12	1.81	5.5	8.48	−0.212	−0.218	−0.067	0.04	−0.99
Bushehr	−0.333	−1.39	−1.02	−2.11	−1.2	−0.20	−2.54	−3.15	−2.22	1.66	−1.15	0.0342	−0.187	−2.91	−7.19
Ilam	−1	−2.38	−2.7	−2.08	21.57	−4.52	−3.33	−2.21	−3	23.75	−9.61	−50.93	−69.99	−14.81	26.34
Kermanshah	3.3×10^{-6}	−9	−11	$−4.9 \times 10^{-7}$	4	−11	−6.66	−7.01	−5	3	−30.42	−20.62	−43.5	−54.5	−76.1
Khorramabad	−25	−10	2.5	−39.9	−5	−17.5	−5	12.5	−40	45	−20.11	−15.73	5	21.81	−7.51
Sanandaj	0.322	0.6	0.833	1.8	0.5	0.97	1.7	2.27	2.78	3.72	27.95	−10.36	−24.6	−20.94	−47.7
Shahrekord	2.5	1.36	1.76	0.6	−1	2.66	2.28	1.25	1.2	1.42	−1.83	−31.1	−35.31	−56.15	−22.58
Yasuj	−1.66	−1.5	0.937	$−5.7 \times 10^{-9}$	−4	−1.07	1.56	1.87	4.83	−10.2	−141.1	−179	−58.91	−68.16	−71.39
Arak	−0.625	−0.769	1.052	2.619	0.8	−1.5	$−2 \times 10^{-7}$	1.4	0.25	3×10^{-7}	0.09	−0.75	−0.151	−0.894	−1.87
Birjand	0.669	0.357	0.357	$−2.03 \times 10^{-8}$	−1	1.6	0.833	0.466	0.56	1.25	−0.267	−0.078	−0.543	−0.305	0.111
Esfahan	1	1.4×10^{-7}	−1.5	−0.62	2.6×10^{-7}	1	1.11	−0.93	0.933	0.66	−7.90	−23.3	−16.52	−24.62	−18.33
Hamedan	−0.62	$−9.4 \times 10^{-11}$	5.2×10^{-6}	0.41	0.76	−1.8	2	1.66	1.25	−3.33	−46.05	−25.78	−7.087	−15.54	4.86
Kerman	−0.045	−0.044	−0.067	−15	−0.16	0.25	−0.57	−0.25	$−1 \times 10^{-7}$	−0.71	−12.55	−16.8	−15.5	−18.94	−9.37
Qazvin	−0.45	$−1.5 \times 10^{-7}$	−0.434	−0.909	−2	−1.73	−0.45	6×10^{-7}	2×10^{-8}	0.83	−20.25	−10.79	−17.9	−40.27	−48
Semnan	0.357	$−1.29 \times 10^{-7}$	1.5×10^{-8}	−2	−1.42	−1	−0.87	−1.55	−3	−0.33	−8.28	−23.63	−26.2	−27.76	−31.39
Shiraz	−1.42	−1	−3.84	−7.94	−9.5	1.16	−3.21	−3.75	−8.2	−14	−3.13	−13.44	−41.6	−45.39	−87.3
Tehran	$−1 \times 10^{-7}$	$−2.5 \times 10^{-7}$	−1.53	−1.5	−4.28	−0.5	−0.15	−1.15	−3.33	−5.25	13.38	−8.11	−21.8	−20.39	−16.25
Yazd	$−2.8 \times 10^{-8}$	0.434	0.384	−0.5	−0.714	1	1.22	−0.15	−0.57	−2.1	−3.59	−5.40	−5.92	−8.99	−2.4
Urmia	$−1 \times 10^{-8}$	2.6×10^{-7}	1.33	1.66	5.5	2.5	1.5	0.38	0.28	3.67	−24.11	−9	0.56	−12.42	5.41
Tabriz	−0.937	−0.294	−0.416	−0.555	−1.8	−0.78	−0.5	−0.25	−0.94	−1.66	−33.2	−21.4	−27	−26.95	−12.80
Bandar Anzali	−102.64	−145.7	−196.3	−263.78	−395.18	0.285	0.909	1.38	7.5	12.5	−102.6	−145	−196	−263.7	−395
Gorgan	33.58	44.44	1.94	−12.04	−46.76	1.25	1.27	0.454	−1	1.2×10^{-8}	33.58	44.44	1.94	−12.04	−46.7
Zanjan	−14.90	−16.71	−18.66	−24.46	−19.91	−0.48	−0.227	−0.52	0.626	1	−14.90	−16.71	−18.66	−24.46	−19.91
Zahedan	−4.89	−8.98	−10.35	−13.66	−11.53	−1	−0.5	−1.66	−1	1.66	−4.89	−8.98	−10.35	−13.66	−11.53
Mashhad	−2.27	−5.54	−11.66	−13.32	−26.35	−0.66	−0.37	−1.11	−1.5	−2.62	−2.27	−5.54	−11.66	−13.32	−26.35

The results showed that an increase in the 24-h precipitation at higher air temperatures only in Semnan, Yazd, Tabriz, Shiraz, Tehran, and Kerman (located in arid Central Iran) corresponds to annual precipitation increments.

Generally, extreme precipitation events have become more common since the 1950s in many regions of Iran. Western Iran has witnessed the strongest increases in heavy precipitation events with the temperature rise. An increased temperature enhances the water vapor capacity in the air by 7 percent per degree of warming. As observed in different regions such as Iran, an atmosphere with more moisture can produce more intense precipitation events. However, increases in extreme precipitation have not led to an increase in total precipitation in most parts of Iran. The overall results indicated little evidence (only in Central Iran with an arid climate) that increases in extreme rainfall events at higher temperatures resulted in similar increases in the annual precipitation, with most regions throughout Iran showing decreased annual precipitation with higher temperatures.

4. Conclusions

The present study was designed to understand the spatial and temporal trends in precipitation extremes over Iran. Eleven indices were employed to analyze the spatiotemporal characteristics of extreme rainfall and three indices for air temperature changes during the 1951–2019 period. The Mann–Kendall test and quantile regression method were applied to detect the trend of these indices.

The study region is characterized by many complexities related to geography and topography, where the combination of their effects causes high spatiotemporal variability, making weather forecasting difficult. The annual maximum daily precipitation mostly occurs during late winter in Western and Central Iran. However, there is no dominant season for extreme rainfall occurrence in the other parts of Iran. The upward trends in the frequency and intensity of extreme precipitation have increased the risk of extreme precipitation and flooding events in Iran's central, western, and northern areas. Additionally, the air temperature has increased in most regions of Iran, especially in the central, northern, and southern regions of Iran. Therefore, proper regional and national actions should be taken to cope with the threat of more frequent climate extremes in these regions.

The annual precipitations of the stations located at Urmia Lake, the Caspian Sea, and the Eastern Border Basins have a decreasing trend, while the number of rainy days has an increasing trend, which shows the occurrence of lighter rainfall in these regions. Additionally, by increasing the elevation, the annual maximum 24-h precipitation occurs from the fall season to winter (especially late winter). The present study shows an increase in extreme precipitation in the central and western parts of Iran, even in areas where the average annual rainfall has a downward trend. However, our study reveals that not only does the trend of the extreme rainfall depend on global and regional settings, but also, it is highly influenced by the local geographical characteristics. The changes in precipitation extremes over Iran are affected by elevation changes, especially in spatial changes, but these effects have no statistical significance. Therefore, further work needs to be carried out to address this issue.

The application of quantile regression for extreme precipitation of the 90th percentile indicated little evidence to suggest the general positive scaling of the maximum 3-h and 24-h of precipitation over Iran, and a slight rise was replicated in the annual precipitation. In fact, most regions over Iran scaled negatively, implying a reduction in the annual precipitation at higher temperatures. If such historical sensitivities are continued in the future, it would be expected that only the most extreme precipitation would increase, while the annual precipitation would decrease in a large part of Iran. References [69–73] are cited in Supplementary Materials.

References

1. Balling, R.C.; Keikhosravi Kiany, M.S.; Sen Roy, S.; Khoshhal, J. Trends in Extreme Precipitation Indices in Iran: 1951–2007. *Adv. Meteorol.* **2016**, *2016*, 2456809. [CrossRef]
2. Zwiers, F.W.; Alexander, L.V.; Hegerl, G.C.; Knutson, T.R.; Kossin, J.P.; Naveau, P.; Nicholls, N.; Schär, C.; Seneviratne, S.I.; Zhang, X. Climate Extremes: Challenges in Estimating and Understanding Recent Changes in the Frequency and Intensity of Extreme Climate and Weather Events. In *Climate Science for Serving Society: Research, Modeling and Prediction Priorities*; Asrar, G.R., Hurrell, J.W., Eds.; Springer: Dordrecht, The Netherlands, 2013; pp. 339–389.
3. Zhang, Q.; Xu, C.-Y.; Tao, H.; Jiang, T.; Chen, Y.D. Climate changes and their impacts on water resources in the arid regions: A case study of the Tarim River basin, China. *Stoch. Environ. Res. Risk Assess.* **2010**, *24*, 349–358. [CrossRef]
4. Zhang, Q.; Xu, C.-Y.; Zhang, Z.; Chen, Y.D.; Liu, C.-l.; Lin, H. Spatial and temporal variability of precipitation maxima during 1960–2005 in the Yangtze River basin and possible association with large-scale circulation. *J. Hydrol.* **2008**, *353*, 215–227. [CrossRef]
5. Wright, D.B.; Samaras, C.; Lopez-Cantu, T. Resilience to Extreme Rainfall Starts with Science. *Bull. Am. Meteorol. Soc.* **2021**, *102*, E808–E813. [CrossRef]
6. Asfaw, A.; Simane, B.; Hassen, A.; Bantider, A. Variability and time series trend analysis of rainfall and temperature in northcentral Ethiopia: A case study in Woleka sub-basin. *Weather. Clim. Extrem.* **2018**, *19*, 29–41. [CrossRef]
7. Bohlinger, P.; Sorteberg, A. A comprehensive view on trends in extreme precipitation in Nepal and their spatial distribution. *Int. J. Climatol.* **2018**, *38*, 1833–1845. [CrossRef]
8. Hajani, E.; Rahman, A.; Ishak, E. Trends in extreme rainfall in the state of New South Wales, Australia. *Hydrol. Sci. J.* **2017**, *62*, 2160–2174. [CrossRef]
9. Jiang, P.; Yu, Z.; Gautam, M.R.; Acharya, K. The Spatiotemporal Characteristics of Extreme Precipitation Events in the Western United States. *Water Resour. Manag.* **2016**, *30*, 4807–4821. [CrossRef]
10. Jung, I.-W.; Bae, D.-H.; Kim, G. Recent trends of mean and extreme precipitation in Korea. *Int. J. Climatol.* **2011**, *31*, 359–370. [CrossRef]
11. Kunkel, K.E.; Easterling, D.R.; Redmond, K.; Hubbard, K. Temporal variations of extreme precipitation events in the United States: 1895–2000. *Geophys. Res. Lett.* **2003**, *30*, 291–305. [CrossRef]
12. Li, W.; Duan, L.; Luo, Y.; Liu, T.; Scharaw, B. Spatiotemporal Characteristics of Extreme Precipitation Regimes in the Eastern Inland River Basin of Inner Mongolian Plateau, China. *Water* **2018**, *10*, 35. [CrossRef]
13. Machekposhti, K.H.; Sedghi, H.; Telvari, A.; Babazadeh, H. Modeling climate variables of rivers basin using time series analysis (case study: Karkheh River basin at Iran). *Civ. Eng. J.* **2018**, *4*, 78–92. [CrossRef]
14. Mishra, A.K.; Singh, V.P. Changes in extreme precipitation in Texas. *J. Geophys. Res. Atmos.* **2010**, *115*, 29. [CrossRef]
15. Peng, Y.; Zhao, X.; Wu, D.; Tang, B.; Xu, P.; Du, X.; Wang, H. Spatiotemporal Variability in Extreme Precipitation in China from Observations and Projections. *Water* **2018**, *10*, 1089. [CrossRef]
16. Rajeevan, M.; Bhate, J.; Jaswal, A.K. Analysis of variability and trends of extreme rainfall events over India using 104 years of gridded daily rainfall data. *Geophys. Res. Lett.* **2008**, *35*, 6. [CrossRef]
17. Wan, L.; Zhang, X.P.; Ma, Q.; Zhang, J.J.; Ma, T.Y.; Sun, Y.P. Spatiotemporal characteristics of precipitation and extreme events on the Loess Plateau of China between 1957 and 2009. *Hydrol. Process.* **2014**, *28*, 4971–4983. [CrossRef]

18. Zhai, P.; Zhang, X.; Wan, H.; Pan, X. Trends in Total Precipitation and Frequency of Daily Precipitation Extremes over China. *J. Clim.* **2005**, *18*, 1096–1108. [CrossRef]

19. Donat, M.G.; Lowry, A.L.; Alexander, L.V.; O'Gorman, P.A.; Maher, N. More extreme precipitation in the world's dry and wet regions. *Nat. Clim. Change* **2016**, *6*, 508–513. [CrossRef]

20. Craig, C.A.; Feng, S. A temporal and spatial analysis of climate change, weather events, and tourism businesses. *Tour. Manag.* **2018**, *67*, 351–361. [CrossRef]

21. Mahmood, R.; Jia, S.; Zhu, W. Analysis of climate variability, trends, and prediction in the most active parts of the Lake Chad basin, Africa. *Sci. Rep.* **2019**, *9*, 6317. [CrossRef]

22. Nkemelang, T.; New, M.; Zaroug, M. Temperature and precipitation extremes under current, 1.5 °C and 2.0 °C global warming above pre-industrial levels over Botswana, and implications for climate change vulnerability. *Environ. Res. Lett.* **2018**, *13*, 065016. [CrossRef]

23. Tolika, K.; Anagnostopoulou, C.; Velikou, K.; Vagenas, C. A comparison of the updated very high resolution model RegCM3_10km with the previous version RegCM3_25km over the complex terrain of Greece: Present and future projections. *Theor. Appl. Climatol.* **2016**, *126*, 715–726. [CrossRef]

24. Groisman, P.Y.; Knight, R.W.; Karl, T.R. Heavy Precipitation and High Streamflow in the Contiguous United States: Trends in the Twentieth Century. *Bull. Am. Meteorol. Soc.* **2001**, *82*, 219–246. [CrossRef]

25. Vincent, L.A.; Mekis, É. Changes in Daily and Extreme Temperature and Precipitation Indices for Canada over the Twentieth Century. *Atmosphere-Ocean* **2006**, *44*, 177–193. [CrossRef]

26. Min, S.-K.; Zhang, X.; Zwiers, F.W.; Hegerl, G.C. Human contribution to more-intense precipitation extremes. *Nature* **2011**, *470*, 378–381. [CrossRef]

27. Westra, S.; Alexander, L.V.; Zwiers, F.W. Global Increasing Trends in Annual Maximum Daily Precipitation. *J. Clim.* **2013**, *26*, 3904–3918. [CrossRef]

28. Westra, S.; Fowler, H.J.; Evans, J.P.; Alexander, L.V.; Berg, P.; Johnson, F.; Kendon, E.J.; Lenderink, G.; Roberts, N.M. Future changes to the intensity and frequency of short-duration extreme rainfall. *Rev. Geophys.* **2014**, *52*, 522–555. [CrossRef]

29. Ahani, H.; Kherad, M.; Kousari, M.R.; Rezaeian-Zadeh, M.; Karampour, M.A.; Ejraee, F.; Kamali, S. An investigation of trends in precipitation volume for the last three decades in different regions of Fars province, Iran. *Theor. Appl. Climatol.* **2012**, *109*, 361–382. [CrossRef]

30. Farhangi, M.; Kholghi, M.; Chavoshian, S.A. Rainfall trend analysis of hydrological subbasins in Western Iran. *J. Irrig. Drain. Eng.* **2016**, *3*, 70–73. [CrossRef]

31. Hekmatzadeh, A.A.; Kaboli, S.; Torabi Haghighi, A. New indices for assessing changes in seasons and in timing characteristics of air temperature. *Theor. Appl. Climatol.* **2020**, *140*, 1247–1261. [CrossRef]

32. Kaboli, S.; Hekmatzadeh, A.A.; Darabi, H.; Haghighi, A.T. Variation in physical characteristics of rainfall in Iran, determined using daily rainfall concentration index and monthly rainfall percentage index. *Theor. Appl. Climatol.* **2021**, *144*, 507–520. [CrossRef]

33. Modarres, R.; de Paulo Rodrigues da Silva, V. Rainfall trends in arid and semi-arid regions of Iran. *J. Arid Environ.* **2007**, *70*, 344–355. [CrossRef]

34. Modarres, R.; Sarhadi, A. Rainfall trends analysis of Iran in the last half of the twentieth century. *J. Geophys. Res. Atmos.* **2009**, *114*, 9. [CrossRef]

35. Mohammadi, B. Trend Analysis of annual rainfall over Iran. *Geogr. Environ. Plan.* **2011**, *22*, 95–106.

36. Raziei, T.; Arasteh, P.D.; Saghafian, B. Annual rainfall trend in arid and semi-arid regions of Iran. In Proceedings of the ICID 21st European Regional Conference, Frankfurt, Germany; Slubice, Polan, 15–19 May 2005; pp. 15–19.

37. Soltani, S.; Saboohi, R.; Yaghmaei, L. Rainfall and rainy days trend in Iran. *Clim. Change* **2012**, *110*, 187–213. [CrossRef]

38. Tabari, H.; Talaee, P.H. Temporal variability of precipitation over Iran: 1966–2005. *J. Hydrol.* **2011**, *396*, 313–320. [CrossRef]

39. Alijani, B. Time series analysis of daily rainfall variability and extreme events. In Proceedings of the 10th International Meeting on Statistical Climatology, Beijing, China, 20 August 2007.

40. Ma, S.; Zhou, T.; Dai, A.; Han, Z. Observed Changes in the Distributions of Daily Precipitation Frequency and Amount over China from 1960 to 2013. *J. Clim.* **2015**, *28*, 6960–6978. [CrossRef]

41. Durocher, M.; Burn, D.H.; Mostofi Zadeh, S.; Ashkar, F. Estimating flood quantiles at ungauged sites using nonparametric regression methods with spatial components. *Hydrol. Sci. J.* **2019**, *64*, 1056–1070. [CrossRef]

42. Ahmed, K.; Sachindra, D.A.; Shahid, S.; Iqbal, Z.; Nawaz, N.; Khan, N. Multi-model ensemble predictions of precipitation and temperature using machine learning algorithms. *Atmos. Res.* **2020**, *236*, 104806. [CrossRef]

43. Douglas, E.M.; Vogel, R.M.; Kroll, C.N. Trends in floods and low flows in the United States: Impact of spatial correlation. *J. Hydrol.* **2000**, *240*, 90–105. [CrossRef]

44. Yue, S.; Pilon, P.; Cavadias, G. Power of the Mann–Kendall and Spearman's rho tests for detecting monotonic trends in hydrological series. *J. Hydrol.* **2002**, *259*, 254–271. [CrossRef]

45. Partal, T.; Kahya, E. Trend analysis in Turkish precipitation data. *Hydrol. Process.* **2006**, *20*, 2011–2026. [CrossRef]

46. Tabari, H.; Marofi, S. Changes of Pan Evaporation in the West of Iran. *Water Resour. Manag.* **2011**, *25*, 97–111. [CrossRef]

47. Mann, H.B. Nonparametric Tests Against Trend. *Econometrica* **1945**, *13*, 245–259. [CrossRef]

48. Kendal, M. *Rank Correlation Methods*; Charles Griffin: London, UK, 1975.

49. Yue, S.; Pilon, P. A comparison of the power of the *t* test, Mann-Kendall and bootstrap tests for trend detection/Une comparaison de la puissance des tests t de Student, de Mann-Kendall et du bootstrap pour la détection de tendance. *Hydrol. Sci. J.* **2004**, *49*, 21–37. [CrossRef]

50. von Storch, H.; Navarra, A. *Analysis of Climate Variability: Applications of Statistical Techniques: Proceedings of an Autumn School Organized by the Commision of the European Community on Elba from October 30 to November 6, 1993*; Springer: Berlin/Heidelberg, Germany, 1995; Volume 2.

51. Kendall, M.G.; Stuart, A.J.L. *The Advanced Theory of Statistics*; Charles Griffin & Co.: London, UK, 1968; Volume 3.

52. Sen, P.K. Estimates of the Regression Coefficient Based on Kendall's Tau. *J. Am. Stat. Assoc.* **1968**, *63*, 1379–1389. [CrossRef]

53. Chamaillé-Jammes, S.; Fritz, H.; Murindagomo, F. Detecting climate changes of concern in highly variable environments: Quantile regressions reveal that droughts worsen in Hwange National Park, Zimbabwe. *J. Arid Environ.* **2007**, *71*, 321–326. [CrossRef]

54. Malekinezhad, H.; Zare-Garizi, A. Regional frequency analysis of daily rainfall extremes using L-moments approach. *Atmósfera* **2014**, *27*, 411–427. [CrossRef]

55. Raziei, T.; Daryabari, J.; Bordi, I.; Modarres, R.; Pereira, L.S. Spatial patterns and temporal trends of daily precipitation indices in Iran. *Clim. Chang.* **2014**, *124*, 239–253. [CrossRef]

56. Dhorde, A.G.; Zarenistanak, M.; Kripalani, R.H.; Preethi, B. Precipitation analysis over southwest Iran: Trends and projections. *Meteorol. Atmos. Phys.* **2014**, *124*, 205–216. [CrossRef]

57. Alavinia, S.H.; Zarei, M. Analysis of spatial changes of extreme precipitation and temperature in Iran over a 50-year period. *Int. J. Climatol.* **2021**, *41*, E2269–E2289. [CrossRef]

58. Rahimi, M.; Fatemi, S.S. Mean versus Extreme Precipitation Trends in Iran over the Period 1960–2017. *Pure Appl. Geophys.* **2019**, *176*, 3717–3735. [CrossRef]

59. Fathian, F.; Ghadami, M.; Haghighi, P.; Amini, M.; Naderi, S.; Ghaedi, Z. Assessment of changes in climate extremes of temperature and precipitation over Iran. *Theor. Appl. Climatol.* **2020**, *141*, 1119–1133. [CrossRef]

60. Rahimzadeh, F.; Asgari, A.; Fattahi, E. Variability of extreme temperature and precipitation in Iran during recent decades. *Int. J. Climatol.* **2009**, *29*, 329–343. [CrossRef]

61. Asgari, A.; Rahimzadeh, F.; Mohammadian, N.; Fattahi, E. Trend Analysis of Extreme Precipitation Indices Over Iran. *Iran-Water Resour. Res.* **2007**, *3*, 42–55.

62. Alpert, P.; Ben-Gai, T.; Baharad, A.; Benjamini, Y.; Yekutieli, D.; Colacino, M.; Diodato, L.; Ramis, C.; Homar, V.; Romero, R.; et al. The paradoxical increase of Mediterranean extreme daily rainfall in spite of decrease in total values. *Geophys. Res. Lett.* **2002**, *29*, 31-1–31-4. [CrossRef]

63. Ahmadi, F.; Nazeri Tahroudi, M.; Mirabbasi, R.; Khalili, K.; Jhajharia, D. Spatiotemporal trend and abrupt change analysis of temperature in Iran. *Meteorol. Appl.* **2018**, *25*, 314–321. [CrossRef]

64. Saboohi, R.; Soltani, S.; Khodagholi, M. Trend analysis of temperature parameters in Iran. *Theor. Appl. Climatol.* **2012**, *109*, 529–547. [CrossRef]

65. Murray, V.; Ebi, K.L. IPCC Special Report on Managing the Risks of Extreme Events and Disasters to Advance Climate Change Adaptation (SREX). *J. Epidemiol. Community Health* **2012**, *66*, 759. [CrossRef]

66. Groisman, P.Y.A.; Karl, T.R.; Easterling, D.R.; Knight, R.W.; Jamason, P.F.; Hennessy, K.J.; Suppiah, R.; Page, C.M.; Wibig, J.; Fortuniak, K.; et al. Change. In *Weather and Climate Extremes: Changes, Variations and a Perspective from the Insurance Industry*; Karl, T.R., Nicholls, N., Ghazi, A., Eds.; Springer: Dordrecht, The Netherlands, 1999; pp. 243–283.

67. Degefu, M.A.; Bewket, W. Variability and trends in rainfall amount and extreme event indices in the Omo-Ghibe River Basin, Ethiopia. *Reg. Environ. Change* **2014**, *14*, 799–810. [CrossRef]

68. Porto de Carvalho, J.R.; Assad, E.D.; de Oliveira, A.F.; Silveira Pinto, H. Annual maximum daily rainfall trends in the Midwest, southeast and southern Brazil in the last 71 years. *Weather Clim. Extrem.* **2014**, *5–6*, 7–15. [CrossRef]

69. Ghenim, A.N.; Megnounif, A. Variability and Trend of Annual Maximum Daily Rainfall in Northern Algeria. *Int. J. Geophys.* **2016**, *2016*, 6820397. [CrossRef]

70. Chen, F.; Chen, H.; Yang, Y. Annual and seasonal changes in means and extreme events of precipitation and their connection to elevation over Yunnan Province, China. *Quat. Int.* **2015**, *374*, 46–61. [CrossRef]

71. Guan, Y.; Zheng, F.; Zhang, X.; Wang, B. Trends and variability of daily precipitation and extremes during 1960–2012 in the Yangtze River Basin, China. *Int. J. Climatol.* **2017**, *37*, 1282–1298. [CrossRef]

72. Mei, C.; Liu, J.; Chen, M.-T.; Wang, H.; Li, M.; Yu, Y. Multi-decadal spatial and temporal changes of extreme precipitation patterns in northern China (Jing-Jin-Ji district, 1960–2013). *Quat. Int.* **2018**, *476*, 1–13. [CrossRef]

73. Zhang, D.; Wang, W.; Liang, S.; Wang, S. Spatiotemporal Variations of Extreme Precipitation Events in the Jinsha River Basin, Southwestern China. *Adv. Meteorol.* **2020**, *2020*, 3268923. [CrossRef]